PHOTONICS Research

Highly efficient ultraviolet high-harmonic generation from epsilon-near-zero indium tin oxide films

Wendong Tian,[1] Fei Liang,[1,2] Dazhi Lu,[1] Haohai Yu,[1,3] and Huaijin Zhang[1]

[1]State Key Laboratory of Crystal Materials and Institute of Crystal Materials, Shandong University, Jinan 250100, China
[2]e-mail: liangfei@sdu.edu.cn
[3]e-mail: haohaiyu@sdu.edu.cn

Received 12 November 2020; revised 21 December 2020; accepted 31 December 2020; posted 5 January 2021 (Doc. ID 414570); published 11 February 2021

High-harmonic generation in the ultraviolet region is promising for wireless technology used for communications and sensing. However, small high-order nonlinear coefficients prevent us from obtaining high conversion efficiency and functional photonic devices. Here, we show highly efficient ultraviolet harmonic generation extending to the fifth order directly from an epsilon-near-zero indium tin oxide (ITO) film. The real part of the annealed ITO films was designed to reach zero around 1050 nm, matching with the central wavelength of an Yb-based fiber laser, and the internal driving electric field was extremely enhanced. A high energy conversion efficiency of 10^{-4} and 10^{-6} for 257.5 nm (fourth-order) and 206 nm (fifth-order) ultraviolet harmonic generation was obtained, which is at least 2 orders of magnitude higher than early reports. Our results demonstrate a new route for overcoming the inefficiency problem and open up the possibilities of compact solid-state high-harmonic generation sources at nanoscale.

https://doi.org/10.1364/PRJ.414570

1. INTRODUCTION

Nonlinear optical harmonic generation is a typical strong-field physical process, which requires strong electric field intensity to trigger light–matter interaction [1–3]. For example, second-order nonlinearity, including second-harmonic generation (SHG), optical parametric oscillation (OPO), and sum frequency generation (SFG), extends the laser spectral range from visible to mid-infrared, and even the terahertz (THz) region [4–6]. Furthermore, high-order harmonic generation (HHG), producing coherent ultraviolet (UV) light, extreme-ultraviolet (EUV) light, and soft X-ray sources [7], is gaining increasing attention for space-to-space communication, laser manufacturing, and attosecond physics [8–10]. The realization of compact and reliable UV coherent sources at nanoscale is now opening the door to industrial and scientific applications with improved reliability, better material compatibility, and greater resolution owing to their shorter wavelengths, such as wafer scribing, photolithography, and flow cytometry [11,12].

Since the 1980s, HHG in the UV and EUV region has been studied in atomic gases and bulk crystals for decades [13]. However, the conversion efficiency is very low ($<10^{-6}$ for the fifth and higher orders) [14]. According to nonlinear optical principles [3], the lowest-order induced polarization $P^{(2)}$ would be comparable to the linear polarization $P^{(1)}$ when the amplitude of the applied field E is of the order of the atomic electric field strength E_{at} ($\sim 5.1 \times 10^{11}$ V/m). For condensed matter, first-order susceptibility $\chi^{(1)}$ is of the order of unity; hence, second-order susceptibility $\chi^{(2)}$ would be expected on the order of $1/E_{\mathrm{at}}$, that is, $\sim 10^{-12}$ m/V. For higher-order nonlinearity, the $\chi^{(n)}$ susceptibility would be reduced by scaling of $(1/E_{\mathrm{at}})^n$, and the response is too inefficient to be detectable. Therefore, it remains a great challenge to obtain direct UV HHG with high conversion efficiency, especially pumped by the commercial light sources, e.g., the Ti:sapphire laser ($\lambda \sim 800$ nm) and Yb-based fiber laser ($\lambda \sim 1030$ nm).

Clearly, a strong driving field (external and internal) is the sufficient condition for improving the conversion efficiency. By applying an external mid-infrared femtosecond laser with ultra-high peak power, direct HHG has been realized in ZnO crystal (pump source, 3.2–3.7 μm, up to 27th order) [15] and MoS_2 monolayer (pump source, 4.1 μm, up to 13th order) [16]. Besides, another strategy to avoid the inefficiency problem is the enhancement of the internal electric field. This could be realized in some special nonlinear media with a refractive index (permittivity epsilon) for the interacting wavelengths near zero [17]. Based on Maxwell's equations and boundary conditions of the electric displacement vector, the epsilon-near-zero (ENZ) effect can greatly boost the internal laser field, which

is appealing for highly efficient nonlinear harmonic generation. As presented in artificial metamaterials with zero refractive index at 1330 nm [18], the conversion efficiency of the third-order four-wave mixing (FWM) was increased to 10^{-5}. Moreover, the ENZ effect is also available in some semiconductor films with tunable ENZ wavelength λ_{ENZ} by doping or annealing [19,20], such as Sn:In_2O_3 (ITO), Al:ZnO (AZO), and Y:CdO. To our best knowledge, only Yang *et al.* reported a UV seventh-order harmonic wave ($\lambda \sim 297$ nm) from In-doped CdO film pumped by a complex Ti:sapphire optical parametric amplifier (OPA) system at 2080 nm [21], in which the energy conversion efficiency is on the order of 10^{-10}.

Herein, we reported UV nonlinear harmonic generation from indium tin oxide (ITO) film epitaxially grown on a silicon substrate by magnetron sputtering. ITO films were selected because their carrier concentration could be adjusted by annealing treatment, and the real part of its permittivity reaches zero around 1050 nm, thus matching with the central wavelength of the Yb-based fiber laser without additional nonlinear conversion [22]. Using a 1030 nm femtosecond laser, odd- and even-order harmonic waves up to fifth order (second, third, fourth, and fifth) were observed, corresponding to the shortest UV wavelength at 206 nm, with an unprecedented high conversion efficiency of 10^{-6} for the fifth order. This work opens new functionalities and applications of ENZ media in nonlinear optics [23,24], such as high-order frequency conversion and entangled photon sources directly pumped by a Ti:sapphire laser and Yb-fiber laser.

2. FABRICATION AND CHARACTERIZATION OF THE ITO SAMPLE

ITO film with doping Sn concentration of 1% (atomic fraction) was prepared by a magnetron sputtering technique on a silicon substrate. Annealing treatment at 750°C for 12 h was adopted to improve ITO film quality and regulate its carrier concentration, as well as ENZ wavelength. The X-ray diffraction pattern was recorded in the 2θ range of 10°–70° with a scanning speed of 1° per minute. As shown in Fig. 1(a), ITO film exhibits strong diffraction peaks at 21.5°, 30.6°, 35.4°, 51.1°, and 60.6°, which is consistent with standard power diffraction file (PDF) card of In_2O_3, corresponding to the (211), (222), (400), (440), and (622) directions of crystal structure. Notably, owing to a smaller radius of doping Sn atom (1.41 Å versus 1.63 Å, 1 Å = 0.1 nm), the peak position of ITO film is a slight redshift contrast to In_2O_3 [see inset graph in Fig. 1(a)]. Meanwhile, strong diffraction peak intensities illustrate that our prepared ITO film enables good crystallinity. No additional peaks relating to any impurity are ascertained, hence specifying high phase purity of the film.

The morphology and thickness of ITO film were characterized by scanning electron microscopy (SEM) and atomic force microscopy (AFM). In Fig. 1(b), the SEM image of oblique ITO film is rough and granular. This imperfectly flat surface is favorable for following nonlinear optical experiments as to avoid zero electric field component along the z direction and reduced interaction strength between the incident light electric field and the ITO surface [25]. Figure 1(c) demonstrates that the thickness of ITO film is around 103 nm. It is worth emphasizing that this is shorter than coherent length (tens of micrometers) of harmonic generation in nonlinear process. Therefore, phase mismatch along the forward direction is nearly negligible. In addition, Raman spectroscopy was measured with a 532 nm excitation laser in Fig. 1(d). There are five strong Raman active modes with Raman shifts at 305, 364, 405, 492, and 627 cm^{-1}, respectively, which is consistent with previous reports [26].

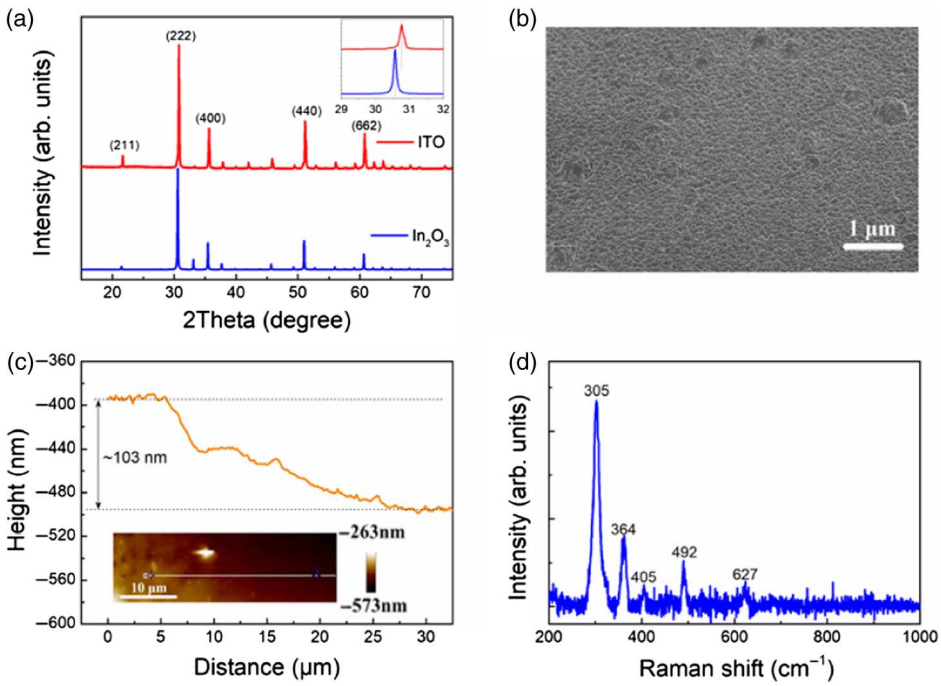

Fig. 1. (a) X-ray diffraction (XRD) pattern of ITO film; the standard diffraction of In_2O_3 is plotted as comparison. The inset graph is the enlargement from 29° to 32°. (b) SEM image of the ITO film. (c) AFM characterization of ITO film. (d) Raman spectrum of ITO film.

3. PERMITTIVITY AND HIGH-HARMONIC GENERATION IN THE ITO FILM

ITO film is a common transparent conducting oxide film with adjustable carrier concentration and exhibits near-zero permittivity around the near-infrared region. According to Maxwell's equations and boundary conditions of the electric displacement vector, the reduced permittivity will bring an enhanced electric field, which is favorable to strengthen the light–matter interaction and is appealing for obtaining phase mismatch-free second-order harmonic generation and even HHG.

The frequency dependent complex electric permittivity of ITO, $\varepsilon_{\mathrm{ITO}}$, is described by the Drude model:

$$\varepsilon = \varepsilon_{\infty} - \frac{\omega_p^2}{\omega^2 - i\tau\omega}, \tag{1}$$

where ε_{∞} is the high frequency epsilon, ε_0 is the free space epsilon, ω is the angular frequency of incident photon, $\omega_p = \sqrt{\frac{ne^2}{\varepsilon_0 m^*}}$ is the plasma frequency, $\tau = \frac{e}{\mu m^*}$ is the charge carrier collision rate, e is elementary charge, and m^* is the effective mass of electron for ITO. The carrier concentration n and mobility μ were measured via the Hall effect. As shown in Fig. 2(a), it is obvious that both the real $\mathrm{Re}(\varepsilon)$ and imaginary $\mathrm{Im}(\varepsilon)$ parts of the epsilon become near zero around the wavelength of 1051 nm and the epsilon of ITO film at the wavelength of 1030 nm is $0.16796 + 0.12846i$. This is well matched with commercial Yb-based fiber ultrafast lasers. Meanwhile, the absolute values of $\mathrm{Re}(\varepsilon)$ and $\mathrm{Im}(\varepsilon)$ are below unity from 910 to 1180 nm, namely the ENZ region. According to the boundary conditions of Maxwell's equations, the perpendicular electric fields in the air ($E_{\mathrm{air}-z}$) and ITO ($E_{\mathrm{ITO}-z}$) should follow the relation of $\frac{E_{\mathrm{ITO}-z}}{E_{\mathrm{air}-z}} = \frac{1}{\varepsilon_{\mathrm{ITO}}}$. So, the intensity of E_{ITO} can be increased by 5.95 and 277.5 times at the wavelength of 1030 and 1501 nm [see Fig. 2(b)]. The figure of merit (FOM) of ITO film at 1030 nm is 1.307 [27], which is comparable to other ENZ materials [28].

In the nonlinear optical process, the nth-order electric polarization intensity $P^{(n)}$ depends on the incident light electric field intensity E as follows [3]:

$$P^{(n)} = \varepsilon_0 \chi^{(n)} E^n, \tag{2}$$

where ε_0 is the vacuum epsilon and $\chi^{(n)}$ is the nth-order nonlinear susceptibility. With the extreme enhancement of the light electric field intensity at the ITO film interface [Fig. 2(c)], the induced nonlinear electric polarization intensity will be strongly increased, thereby leading to possible nonlinear HHG at nanoscale films.

The schematic illustration and experimental setup for nonlinear high-harmonic generation are illuminated in Fig. 2(d). A mode-locked femtosecond laser system (central wavelength ~1030 nm, pulse width ~250 fs, and repetition rate ~200 kHz) was focused by a 100× objective to a spot radius of 10 μm. The high-harmonic signals were collected from reflected signals via the same objective using charge-coupled device (CCD) camera, and the respective powers of nth-order harmonics were measured by a powermeter. It is worthy to point out that the light beam

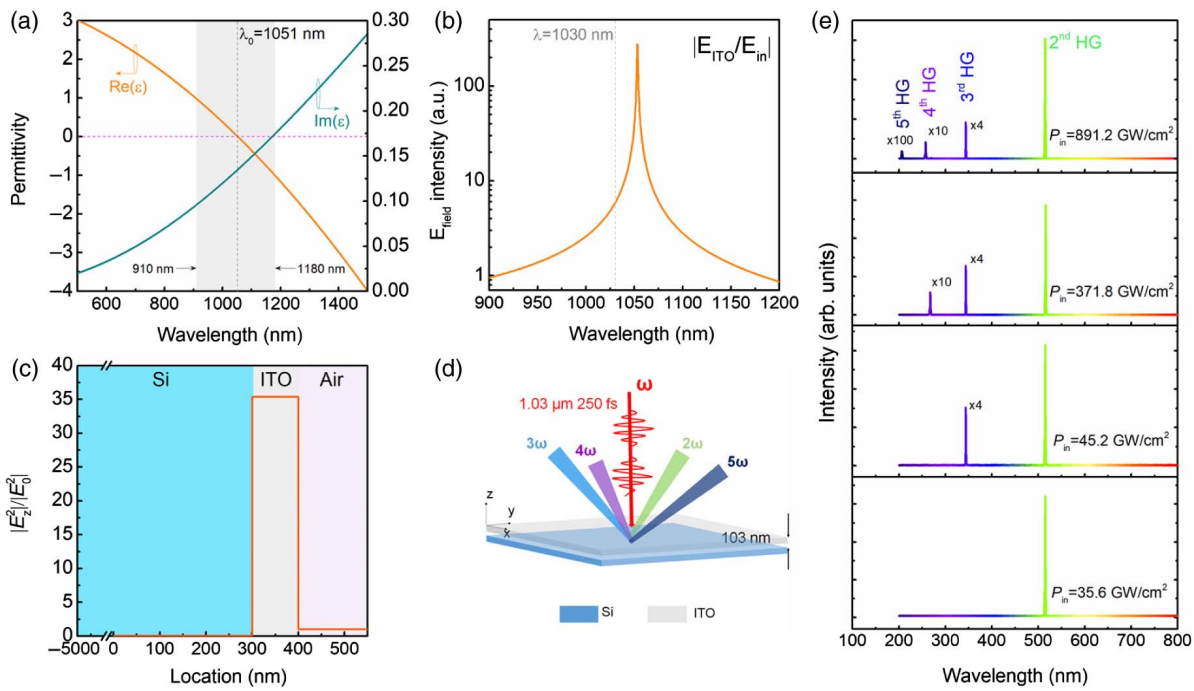

Fig. 2. (a) Calculated real and imaginary parts of the permittivity of ITO film as a function of wavelength. (b) Calculated field enhancements of the ITO film as a function of incident laser wavelength. (c) Calculated field enhancements of the structure as a function of location at 1.03 μm. (d) Schematic of nonlinear harmonic generation on the ENZ sample composed of silicon substrate and ITO film. The pump laser is vertically incident from the ITO side. Notably, the light beam direction of harmonic waves is only a diagrammatic sketch, not the real propagating direction. (e) The harmonic spectrum under different incident pump power densities. The intensity of the third-, fourth-, and fifth-harmonic generation was enlarged for clarity.

direction in Fig. 2(d) is only a diagrammatic sketch, not the real propagating direction of high-harmonic waves.

Figure 2(e) depicts the high-harmonic generation in ITO film pumped by 1030 nm femtosecond laser. Clearly, the second-order harmonic generation was first measured with incident power intensity of 35.6 $\mathrm{GW \cdot cm^{-2}}$, corresponding to a vacuum field strength of 0.52 $\mathrm{V \cdot nm^{-1}}$. With gradually improved pumped intensity, the third-, fourth-, and fifth-harmonic waves start to emerge with excitation intensity at 45.2, 371.8, 891.2 $\mathrm{GW \cdot cm^{-2}}$ (vacuum field strength of 0.58, 1.67, and 2.59 $\mathrm{V \cdot nm^{-1}}$), respectively. The improved excitation threshold for fourth- and fifth-harmonic generation may be attributed to additional absorption of ITO film at 257.5 and 206 nm. Notably, this excitation energy is comparable to the typical intensity used for HHG from bulk or monolayer solids [13]. For instance, 0.5 $\mathrm{TW \cdot cm^{-2}}$ (3.25 μm, ninth order) in zinc oxide [15], and 0.7 $\mathrm{TW \cdot cm^{-2}}$ (4.1 μm, seventh order) in MoS_2 monolayer [16]. Moreover, this excitation intensity is slightly higher than that for ENZ In:CdO film [21] (2.08 μm, ~0.3 $\mathrm{GW \cdot cm^{-2}}$ for the third order and ~0.5 $\mathrm{GW \cdot cm^{-2}}$ for the fifth order), in which the real part of its permittivity crosses zero at a wavelength of 2.09 μm. The excitation intensity for HHG in ITO film would be further reduced when the central wavelength is nearer to 1051 nm due to the large resonant field enhancement.

In order to quantify the second- and third-order susceptibility of the investigated nanolayers, we performed relative measurements with two different reference materials. The spectral range of a broadband fundamental wave with a central wavelength at 1030 nm is plotted in Fig. 3(a). The second-order susceptibility can be determined by measuring the relative SHG intensity between ITO film and GaAs (111) crystal, the known large second-order susceptibility $\chi^{(2)}_{\mathrm{GaAs}}$ of 710 pm/V [29]. For 1030 nm SHG, our experimental measurements indicated that the SHG intensity of ITO film is much higher than that of GaAs, with a ratio of $I^{(2\omega)}_{\mathrm{ITO}}/I^{(2\omega)}_{\mathrm{GaAs}} \approx 4.033$ in Fig. 3(b), when both are pumped by the incident power of 42.2 $\mathrm{GW \cdot cm^{-2}}$. Associated with the SHG theory, the SHG intensity ($I^{(2\omega)}$) can be determined by

$$I^{(2\omega)} \propto \frac{2\omega^2}{c^3 n^2_{(\omega)} n_{(2\omega)} \varepsilon_0} |\chi^{(2)} E^2|^2, \tag{3}$$

where c is the speed of light, n is linear refractive index, ε_0 is the vacuum epsilon, E is the electric field in the sample, and $\chi^{(2)}$ is the second-order susceptibility. Owing to relatively large epsilon ($\varepsilon = 12.2$ at 1030 nm) [30], the electric field E in GaAs decreases to only 1/12.2 of E_{air}. In contrast, the electric field in ITO film is enhanced by 5.95 times at wavelength of 1030 nm, owing to the reduced epsilon of 0.1679. Accordingly, the electric field on ITO film is nearly 73 times stronger than that of GaAs. Therefore, it can be deduced that the absolute value $\chi^{(2)}$ of ITO film is 0.273 $\mathrm{pm \cdot V^{-1}}$ at 1030 nm, which is in good agreement with previous studies [31,32] (0.18 $\mathrm{pm \cdot V^{-1}}$ at 1150 nm and 0.1 $\mathrm{pm \cdot V^{-1}}$ at 1064 nm). Clearly, the value of $\chi^{(2)}$ for ITO film is far less than that of GaAs. This strongly demonstrated that the origin of large second-order nonlinear optical response on ITO film is deduced from the boosted electric field in the ENZ region but not increased second-order nonlinear susceptibility.

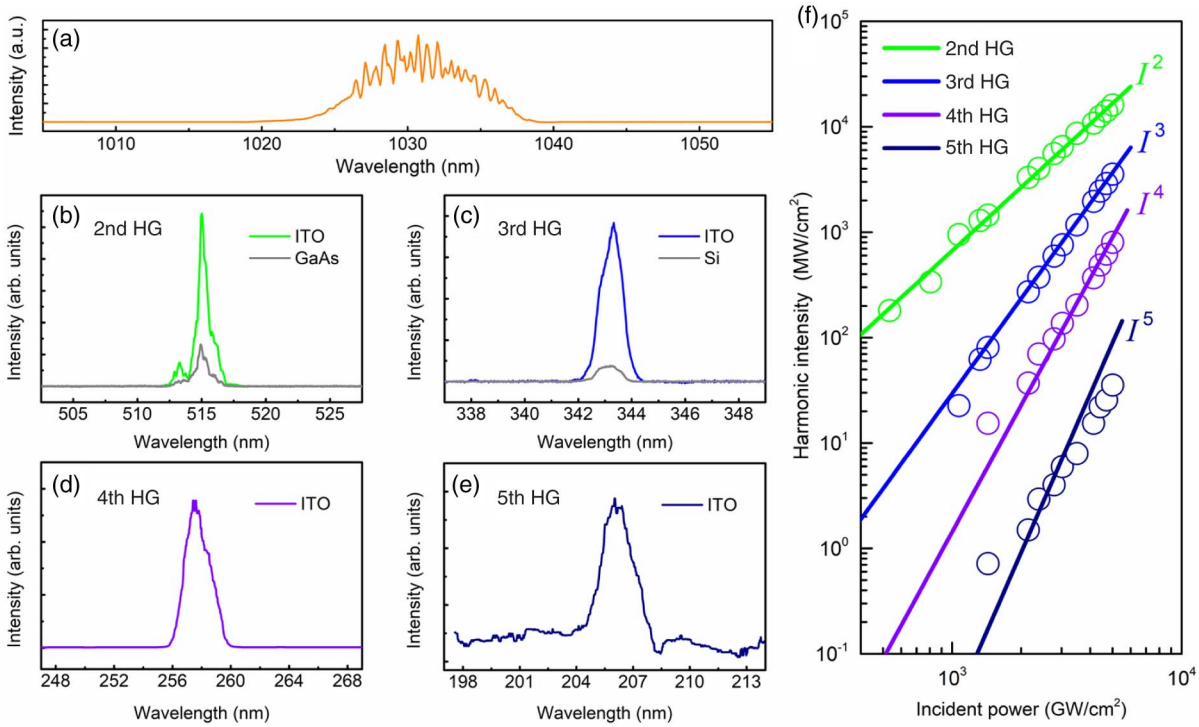

Fig. 3. (a) Spectrum of the fundamental wave. (b) The second-harmonic spectrum of ITO film and GaAs (111) crystal with pump intensity of 42.2 $\mathrm{GW \cdot cm^{-2}}$. (c) The third-harmonic spectrum of ITO film and Si (100) with pump intensity of 51.4 $\mathrm{GW \cdot cm^{-2}}$. (d) The fourth-harmonic and (e) fifth-harmonic spectra of ITO film with pump intensity of 438 and 944 $\mathrm{GW \cdot cm^{-2}}$. (f) The generated harmonic power as a function of incident pump power. Solid lines show the power scaling law I^n and are plotted to guide the eye.

According to a previous report [31], the prepared ITO film is isotropic within in-plane direction (C_∞ symmetry). Accordingly, the polarization measurement shows that second-harmonic intensity is nearly independent on the polarization direction of incident light.

Same as the experimental facility above, the third-harmonic response of ITO film was studied with the wavelength of pump light at 1030 nm and the incident power of 51.4 GW·cm^{-2}. In order to estimate the third-order susceptibility of ITO film, Si (100) wafer was selected as a reference material with a third-order susceptibility of 1.05×10^{-16} m^2·V^{-2} [33]. In Fig. 3(c), the third-harmonic generation intensity of ITO film is 9.42 times stronger than that of Si (100) wafer. According to third-order nonlinear optical theory, the third-harmonic intensity ($I^{(3\omega)}$) can be determined by

$$I^{(3\omega)} \propto \left(\frac{3\omega}{2cn_{(3\omega)}}\right)^2 |\chi^{(3)}E^3|^2, \tag{4}$$

where $\chi^{(3)}$ is the third-order susceptibility. Similar to SHG discussed above, the electric field in Si medium decreases to 1/3.95, due to the epsilon of Si (100) being 3.95 at 1030 nm [34]. Therefore, the internal electric field of ITO film is nearly 23.5 times stronger than that on Si wafer. Taking this enhancement factor into account, the third-order susceptibility $\chi^{(3)}$ of ITO film is determined to be 2.48×10^{-20} m^2·V^{-2}, which is in good agreement with previous studies (2.37×10^{-20} m^2·V^{-2} at 1.9 μm) [35] and 4 orders of magnitude smaller than that of Si wafer. This also confirms that the resonantly boosted electric field brings enhanced third-order nonlinear response. The third-harmonic intensity keeps unchanged with the variation of the polarization angle of incident laser, which is also consistent with in-plane isotropy.

More impressively, due to a strongly enhanced electric field, we also measured direct fourth- and fifth-harmonic generation on ENZ ITO film, which is very rare in common nonlinear optical materials. As shown in Figs. 3(d) and 3(e), the fourth- and fifth-harmonic generation signals are measured by a CCD camera with the incident power of 438 GW·cm^{-2} and 944 GW·cm^{-2}, respectively. When we continue to improve the incident pump intensity, a supercontinuum spectrum from 303 to 945 nm was collected under incident power of 9.56 TW·cm^{-2}. Generally, supercontinuum generation on a surface is a challenging task because the surficial nonlinear optical efficiency is usually limited by finite light–matter interaction length [25]. Benefitting from a greatly enhanced electric field, a high conversion efficiency up to 1.2% is obtained in supercontinuum generation under 29.3 TW·cm^{-2} incident power. It is credible to measure the sixth-, seventh-, and even higher-order harmonic waves, however, beyond the detectable spectral range of our experimental setup.

The output powers of high-harmonic generation are also measured quantitatively. Figure 3(f) shows the harmonic intensity as a function of the excitation intensity, with perfect scaling law I^2, I^3, and I^4 for second-, third-, and fourth-harmonic waves. The fifth-harmonic energy was estimated from the measured fourth-harmonic energy by referring to Fig. 2(e) [21]. Clearly, the fifth-harmonic intensity slightly deviates from fifth-order power law. This could be attributed to two reasons. (i) The fifth-harmonic wave power is too low to be detected by our powermeter. The fluctuation of relative intensity of fourth- and fifth-harmonic waves could bring larger error and power deviation. (ii) Under a strong expiation field, the non-perturbative effect starts to become significant for high-harmonic generation. This case has been reported in many early HHG experiments [11,12,16,21].

The energy conversion efficiency for the second-, third-, fourth-, and fifth-harmonic generation is determined to be around 3.20×10^{-3}, 7.05×10^{-4}, 1.59×10^{-4}, and 7.08×10^{-6},

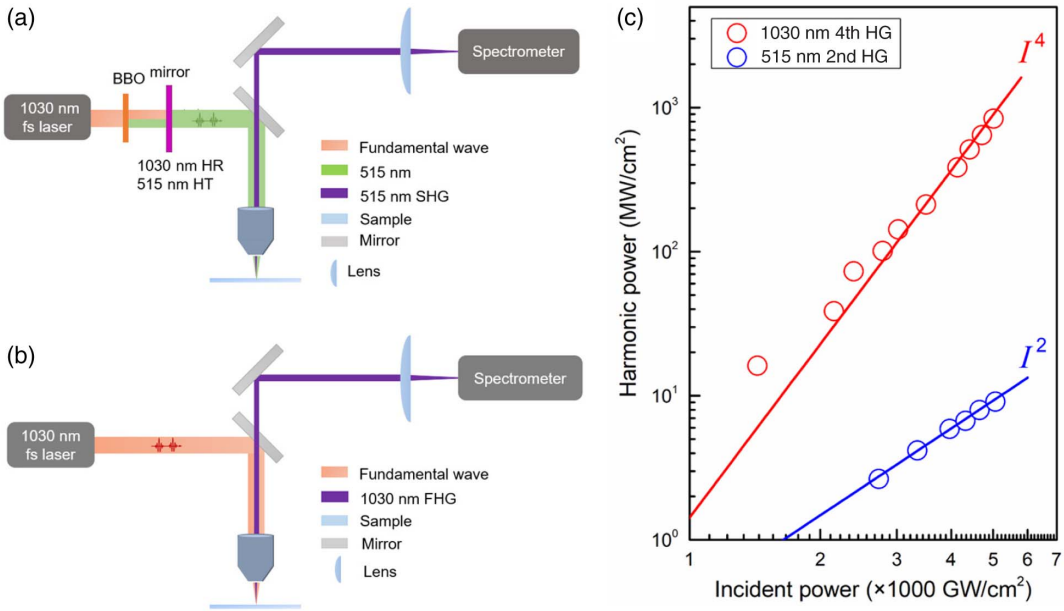

Fig. 4. (a) Experimental setup for 515 nm pumped second-harmonic generation in ITO film. HR and HT represent high reflectivity (>99%) and high transmittance (>95%). (b) Experimental setup for 1030 nm pumped fourth-harmonic generation in ITO film. (c) The second-harmonic power as a function of incident 515 nm pump intensity and the fourth-harmonic power as a function of incident 1030 nm pump intensity.

respectively, under a pump intensity of 5.01 $TW \cdot cm^{-2}$. This efficiency is a strongly improved contrast to typical efficiency ($\sim 10^{-10}$) of second-order harmonic generation on the surfaces [36]. Meanwhile, it is nearly 2 orders of magnitude higher than that in In:CdO film (10^{-5} for the third, 10^{-8} for the fifth, 10^{-10} for the seventh harmonics) [21]. Taking the short interaction length in the ITO film (hundreds of nanometers) into account, this unprecedented efficiency suggests the giant potential of ENZ materials in highly integrated nonlinear optoelectronics.

Finally, we performed another experiment to demonstrate the crucial role of the ENZ effect with two different incident lasers. As shown in Figs. 4(a) and 4(b), the fundamental laser (1030 nm) and the frequency-doubled laser (515 nm) by BBO crystal were used as the incident source. The 515 nm is not located into the ENZ spectral region. As expected, the same 257.5 nm signal, as the direct fourth-harmonic wave of 1030 nm and the second-harmonic wave of 515 nm, exhibits completely different power dependence and excitation energy in two experimental setups. The excitation energy of the second-harmonic wave of 515 nm is 1.76 $TW \cdot cm^{-2}$, which is nearly 5 times higher than that of direct fourth-harmonic wave of 1030 nm, 0.37 $TW \cdot cm^{-2}$. Meanwhile, Fig. 4(c) shows that the energy conversion efficiency of the former is also lower than that of the latter, in which they follow the I^4 and I^2 power law, respectively. This definitely suggests that the ENZ effect is the critical factor to enhance high-harmonic generation. Notably, the generated second-harmonic intensity is below 20 $GW \cdot cm^{-2}$, thereby ruling out the cascaded second-order nonlinearity for 257.5 nm signal under 1030 nm pump light.

Besides ITO film, the ENZ effect is also available in other materials, including ZrN ($\lambda_{ENZ} \sim 485.4$ nm) [37], TiN ($\lambda_{ENZ} \sim 520$ nm) [31], AZO ($\lambda_{ENZ} \sim 1550$ nm) [25], high concentration Y-doped CdO ($\lambda_{ENZ} \sim 5.3$ μm) [38], CdO ($\lambda_{ENZ} \sim 11.3$ μm) [38], and various artificial metamaterials. Especially, the ENZ wavelengths of Au film ($\lambda_{ENZ} \sim 796$ nm) [39] and Ag-SiO_2 multilayer films ($\lambda_{ENZ} \sim 820$–890 nm) [40] are matched to the Ti:sapphire laser. Therefore, this enhanced high-harmonic generation could be obtained in wide spectral range by applying suitable ENZ media. This λ_{ENZ} modulation strategy by annealing treatment is also significant for other nonlinear processes pumped by the Ti:sapphire laser and fiber laser, such as difference frequency generation (DFG), optical rectification (OR), FWM, and THz generation.

4. CONCLUSION

In summary, we reported the UV high-harmonic generation in annealed ITO film for the first time. Pumped by an Yb-based 1030 nm femtosecond laser, odd- and even-order harmonic waves up to fifth order at 206 nm were observed with an unprecedented high conversion efficiency of 10^{-6}. Assisted by the extremely enhanced electric field in ENZ region and tunable ENZ wavelength, ITO film provides a newfangled platform to study nonlinear light–matter interaction within hundreds of nanometers thickness, including strong-field physics and attosecond science. Meanwhile, ITO film is compatible with silicon photonics, which could have further applications in highly integrated nonlinear photonic devices based on nanolayers.

Funding. National Natural Science Foundation of China (51632004, 51772173, 51890863, 51902181, 52002220); Taishan Scholar Foundation of Shandong Province; Future Plans of Young Scholars at Shandong University.

Disclosures. The authors declare no conflicts of interest.

REFERENCES

1. T. H. Maiman, "Stimulated optical radiation in ruby," Nature **187**, 493–494 (1960).
2. P. A. Franken, G. Weinreich, C. W. Peters, and A. E. Hill, "Generation of optical harmonics," Phys. Rev. Lett. **7**, 118–120 (1961).
3. R. W. Boyd, *Nonlinear Optics* (Academic, 2008).
4. C. T. Chen, G. L. Wang, X. Y. Wang, and Z. Y. Xu, "Deep-UV nonlinear optical crystal $KBe_2BO_3F_2$—discovery, growth, optical properties and applications," Appl. Phys. B **97**, 9–25 (2009).
5. V. Petrov, "Frequency down-conversion of solid-state laser sources to the mid-infrared spectral range using non-oxide nonlinear crystals," Prog. Quantum Electron. **42**, 1–106 (2015).
6. D. Yan, Y. Wang, D. Xu, P. Liu, C. Yan, J. Shi, H. Liu, Y. He, L. Tang, J. Feng, J. Guo, W. Shi, K. Zhong, Y. H. Tsang, and J. Yao, "High-average-power, high-repetition-rate tunable terahertz difference frequency generation with GaSe crystal pumped by 2 μm dual-wavelength intracavity KTP optical parametric oscillator," Photon. Res. **5**, 82–87 (2017).
7. F. Krausz and M. Ivanov, "Attosecond physics," Rev. Mod. Phys. **81**, 163–234 (2009).
8. Z. Xu and B. M. Sadler, "Ultraviolet communications: potential and state-of-the-art," IEEE Commun. Mag. **46**, 67–73 (2008).
9. T. Popmintchev, M. C. Chen, D. Popmintchev, P. Arpin, S. Brown, S. Ališauskas, G. Andriukaitis, T. Balčiunas, O. D. Mücke, A. Pugzlys, A. Baltuška, B. Shim, S. E. Schrauth, A. Gaeta, C. Hernández-García, L. Plaja, A. Becker, A. Jaron-Becker, M. M. Murnane, and H. C. Kapteyn, "Bright coherent ultrahigh harmonics in the keV X-ray regime from mid-infrared femtosecond lasers," Science **336**, 1287–1291 (2012).
10. A. J. Uzan, G. Orenstein, A. Jimenez-Galan, C. McDonald, R. E. F. Silva, B. D. Bruner, N. D. Klimkin, V. Blanchet, T. Arusi-Parpar, M. Kruger, A. N. Rubtsov, O. Smirnova, M. Ivanov, B. H. Yan, T. Brabec, and N. Dudovich, "Attosecond spectral singularities in solid-state high-harmonic generation," Nat. Photonics **14**, 183–188 (2020).
11. N. Yoshikawa, T. Tamaya, and K. Tanaka, "High-harmonic generation in graphene enhanced by elliptically polarized light excitation," Science **356**, 736–738 (2017).
12. M. Sivis, M. Taucer, G. Vampa, K. Johnston, A. Staudte, A. Yu. Naumov, D. M. Villeneuve, C. Ropers, and P. B. Corkum, "Tailored semiconductors for high-harmonic optoelectronics," Science **357**, 303–306 (2017).
13. S. Ghimire and D. A. Reis, "High-harmonic generation from solids," Nat. Phys. **15**, 10–16 (2018).
14. S. Ghimire, A. D. DiChiara, E. Sistrunk, G. Ndabashimiye, U. B. Szafruga, A. Mohammad, P. Agostini, L. F. DiMauro, and D. A. Reis, "Generation and propagation of high-order harmonics in crystals," Phys. Rev. A **85**, 043836 (2012).
15. S. Ghimire, A. D. DiChiara, E. Sistrunk, P. Agostini, L. F. DiMauro, and D. A. Reis, "Observation of high-order harmonic generation in a bulk crystal," Nat. Phys. **7**, 138–141 (2010).
16. H. Liu, Y. Li, Y. S. You, S. Ghimire, T. F. Heinz, and D. A. Reis, "High-harmonic generation from an atomically thin semiconductor," Nat. Phys. **13**, 262–265 (2016).
17. M. Z. Alam, I. De Leon, and R. W. Boyd, "Large optical nonlinearity of indium tin oxide in its epsilon-near-zero region," Science **352**, 795–797 (2016).

18. H. Suchowski, K. O'Brien, Z. J. Wong, A. Salandrino, X. B. Yin, and X. Zhang, "Phase mismatch–free nonlinear propagation in optical zero-index materials," Science **342**, 1223–1227 (2013).
19. Y. Wang, A. Capretti, and L. Dal Negro, "Wide tuning of the optical and structural properties of alternative plasmonic materials," Opt. Mater. Express **5**, 2415–2430 (2015).
20. J. Zhao, H. Zhang, X. Zhang, D. Li, H. Lu, and M. Xu, "Abnormal behaviors of Goos–Hänchen shift in hyperbolic metamaterials made of aluminum zinc oxide materials," Photon. Res. **1**, 160–163 (2013).
21. Y. Yang, J. Lu, A. Manjavacas, T. S. Luk, H. Liu, K. Kelley, J.-P. Maria, E. L. Runnerstrom, M. B. Sinclair, S. Ghimire, and I. Brener, "High-harmonic generation from an epsilon-near-zero material," Nat. Phys. **15**, 1022–1026 (2019).
22. Y. Wang, A. C. Overvig, S. Shrestha, R. Zhang, R. Wang, N. Yu, and L. Dal Negro, "Tunability of indium tin oxide materials for mid-infrared plasmonics applications," Opt. Mater. Express **7**, 2727–2739 (2017).
23. I. Liberal and N. Engheta, "Near-zero refractive index photonics," Nat. Photonics **11**, 149–158 (2017).
24. Q. Guo, Y. Cui, Y. Yao, Y. Ye, Y. Yang, X. Liu, S. Zhang, X. Liu, J. Qiu, and H. Hosono, "A solution-processed ultrafast optical switch based on a nanostructured epsilon-near-zero medium," Adv. Mater. **29**, 1700754 (2017).
25. W. Tian, F. Liang, S. Chi, C. Li, H. Yu, H. Zhang, and H. Zhang, "Highly efficient super-continuum generation on an epsilon-near-zero surface," ACS Omega **5**, 2458–2464 (2020).
26. H. Kim, C. M. Gilmore, A. Pique, J. S. Horwitz, H. Mattoussi, H. Murata, Z. H. Kafafi, and D. B. Chrisey, "Electrical, optical and structural properties of indium-tin-oxide thin films for organic light-emitting devices," J. Appl. Phys. **86**, 6451–6461 (1999).
27. V. M. Shalaev, "Optical negative-index metamaterials," Nat. Photonics **1**, 41–48 (2007).
28. G. V. Naik, J. L. Schroeder, X. Ni, A. V. Kildishev, T. D. Sands, and A. Boltasseva, "Titanium nitride as a plasmonic material for visible and near-infrared wavelengths," Opt. Mater. Express **2**, 478–489 (2012).
29. S. Bergfeld and W. Daum, "Second-harmonic generation in GaAs: experiment versus theoretical predictions of $\chi^{(2)}_{xyz}$," Phys. Rev. Lett. **90**, 036801 (2003).
30. J. S. Blakemore, "Semiconducting and other major properties of gallium-arsenide," J. Appl. Phys. **53**, R123–R181 (1982).
31. A. Capretti, Y. Wang, N. Engheta, and L. Dal Negro, "Comparative study of second-harmonic generation from epsilon-near-zero indium tin oxide and titanium nitride nanolayers excited in the near-infrared spectral range," ACS Photon. **2**, 1584–1591 (2015).
32. W. J. Wang, J. H. Xu, X. Liu, Y. Q. Jiang, G. M. Wang, and X. Z. Lu, "Second harmonic generation investigation of indium tin oxide thin films," Thin Solid Films **365**, 116–118 (2000).
33. Y. J. Chen and G. M. Carter, "Measurement of third order nonlinear susceptibilities by surface plasmons," Appl. Phys. Lett. **41**, 307–309 (1982).
34. G. Lin, Y. Chang, E. Liu, H. Kuo, and H. Lin, "Low refractive index Si nanopillars on Si substrate," Appl. Phys. Lett. **90**, 181923 (2007).
35. N. Ueda, H. Kawazoe, Y. Watanabe, M. Takata, M. Yamane, and K. Kubodera, "Third-order nonlinear optical susceptibilities of electroconductive oxide thin films," Appl. Phys. Lett. **59**, 502–503 (1991).
36. C. S. Tian and Y. R. Shen, "Recent progress on sum-frequency spectroscopy," Surf. Sci. Rep. **69**, 105–131 (2014).
37. O. Reshef, I. De Leon, M. Z. Alam, and R. W. Boyd, "Nonlinear optical effects in epsilon-near-zero media," Nat. Rev. Mater. **4**, 535–551 (2019).
38. S. Saha, B. T. Diroll, J. Shank, Z. Kudyshev, A. Dutta, S. N. Chowdhury, T. S. Luk, S. Campione, R. D. Schaller, V. M. Shalaev, A. Boltasseva, and M. G. Wood, "Broadband, high-speed, and large-amplitude dynamic optical switching with yttrium-doped cadmium oxide," Adv. Funct. Mater. **29**, 1908377 (2019).
39. I. De Leon, Z. Shi, A. C. Liapis, and R. W. Boyd, "Measurement of the complex nonlinear optical response of a surface plasmon-polariton," Opt. Lett. **39**, 2274–2277 (2014).
40. R. M. Kaipurath, M. Pietrzyk, L. Caspani, T. Roger, M. Clerici, C. Rizza, A. Ciattoni, A. Di Falco, and D. Faccio, "Optically induced metal-to-dielectric transition in epsilon-near-zero metamaterials," Sci. Rep. **6**, 27700 (2016).